

# Partitioning intensity inhomogeneity colour images via Saliency-based active contour

Muhammad Syukri Mazlin<sup>1</sup>, Abdul Kadir Jumaat<sup>1,2</sup>, Rohana Embong<sup>1</sup>

<sup>1</sup>School of Mathematical Sciences, College of Computing, Informatics and Mathematics, Universiti Teknologi MARA, Shah Alam, Malaysia

<sup>2</sup>Institute for Big Data Analytics and Artificial Intelligence (IBDAAI), Universiti Teknologi MARA, Shah Alam, Malaysia

## Article Info

### Article history:

Received May 30, 2023

Revised Aug 12, 2023

Accepted Sep 6, 2023

### Keywords:

Colour image

Intensity inhomogeneous image

Saliency image map

Selective image segmentation

Variational active contour

## ABSTRACT

Partitioning or segmenting intensity inhomogeneity colour images is a challenging problem in computer vision and image shape analysis. Given an input image, the active contour model (ACM) which is formulated in variational framework is regularly used to partition objects in the image. A selective type of variational ACM approach is better than a global approach for segmenting specific target objects, which is useful for applications such as tumor segmentation or tissue classification in medical imaging. However, the existing selective ACMs yield unsatisfactory outcomes when performing the segmentation for colour (vector-valued) with intensity variations. Therefore, our new approach incorporates both local image fitting and saliency maps into a new variational selective ACM to tackle the problem. The euler-lagrange (EL) equations were presented to solve the proposed model. Thirty combinations of synthetic and medical images were tested. The visual observation and quantitative results show that the proposed model outshines the other existing models by average, with the accuracy of 2.23% more than the compared model and the Dice and Jaccard coefficients which were around 12.78% and 19.53% higher, respectively, than the compared model.

*This is an open access article under the [CC BY-SA](#) license.*



## Corresponding Author:

Abdul Kadir Jumaat

School of Mathematical Sciences, College of Computing, Informatics and Mathematics, Universiti Teknologi MARA and Institute for Big Data Analytics and Artificial Intelligence (IBDAAI), Universiti Teknologi MARA

Kompleks Al-Khawarizmi, 40450 Shah Alam, Selangor, Malaysia

Email: [abdulkadir@tmsk.uitm.edu.my](mailto:abdulkadir@tmsk.uitm.edu.my)

## 1. INTRODUCTION

Image partitioning, also referred to as image segmentation, is a crucial aspect of computer vision and general image processing applications. These applications include medical imaging techniques [1]–[5] and object recognition [6]–[8] where the main objective behind partitioning, is to segment an input image into several objects based on some preset criteria. Because of the massive and crucial uses, notably in the medical sector, this area of study has become well-known and intensively researched and practised by the scholars. Nevertheless, there are several challenges that might arise throughout the segmentation process thereby impacting the precision and effectiveness of the segmentation. In the medical field, one of the prominent issues stems from variations in colour intensity within medical images, which can result from factors like lighting conditions or environmental influences. Various segmentation methods, such as variational and non-variational techniques have been developed. Even if non-variational methods like machine learning and deep learning algorithms get the job done, they need a vast amount of data to function

well, and that data is not always readily available. They are not precise when dealing with limited information which results in less accurate segmentation outcomes. Meanwhile, variational approach which is independent of amount of data applies the calculus of variations to achieve a near optimal segmentation result which is widely used by the researchers for some areas like [9]–[11] and it is proven to be more accurate and efficient as this approach has demonstrated effectiveness in managing diverse characteristics of image groups and offer advanced image processing abilities with superior quality [12].

The most celebrated variational approach is the active contour model (ACM) which can be categorized into edge-based approach and region-based approach. Edge-based approach relies on detecting and segmenting regions of an image based on the edges or boundaries between different regions. This method is very useful in several applications such as object recognition as well as tumors detection in medical imaging such as [13]. Kass *et al.* [14] proposal of the most well-known edge-based ACM uses the explicit snake. The drawback of this method is that it is very sensitive to noise and may not always produce accurate results, especially in cases where the edges in the image are ambiguous or poorly defined. On the other hand, the region-based approach considers texture characteristics, shape and pixel intensities to converge the segmentation contour to the particular targeted object [15] which is more accurate as it makes the model less sensitive to noise.

Both global and selective segmentations are under the purview of the variational region-based ACM. Mumford and Shah [16] is the most popular and has become the state-of-the-art of the variational global ACM. This model is a variational framework for segmenting images with the goal of breaking them up into specific parts by minimizing an energy functional across those regions. However, this model has an issue where it assumes that the boundaries between regions are well-defined and that the image can be represented as a piecewise-constant function. This led to Chan and Vese proposed the Chan and Vese (CV) [17] model where they addressed this limitation by proposing a level-set based formulation of the Mumford and Shah model, which allows for more flexibility in modelling the boundaries between regions. The CV model can handle images with more complex boundaries and regions with various contrast and texture, making it more robust and adaptable to more kinds of images. Although it is proven in producing a prominent result, this model is only applicable to grayscale image and will change automatically to grayscale images for all the colour images that are being tested. To address this limitation, Chan and Sandberg [18] proposed an extension to the Chan-Vese (CV) model, termed the Chan-Sandberg-Vese (CSV) model where it incorporates a more complex region-based term into the energy functional, which allows for each region to have its own intensity distribution and more importantly, the colour pixels. However, both CV and CSV models are not effective in segmenting non-homogeneous intensity images.

Intensity inhomogeneity is a common problem in image segmentation, where the brightness or darkness of an image varies across different regions, making it challenging to accurately identify and separate objects of interest from their background. This variation in intensity in an input image often results in segmentation errors, where objects are incorrectly classified or incomplete. With this problem arises, Li *et al.* [19] has proposed a global ACM namely the local binary fitting (LBF) model which applied the local binary classifier to distinguish between the object and background regions in an image based on their intensities by utilizing two main components: a local binary classifier and a nonparametric intensity model. However, this model may not perform well in images with complex images features, and it is very computationally expensive. Due to that, a model namely the local image fitting (LIF) was introduced by Zhang *et al.* [20] to deal with the drawbacks in LBF model. Subsequently, various works such as Yang *et al.* [21] and Iqbal *et al.* [22] have applied the LIF model idea in their models' formulations.

In addition to using local image energy fitting to enhance the segmentation outcomes for images which the average intensity is not homogeneous, the use of saliency map has caught researchers' attention and interest. Saliency refers to the quality of being noticeable and is used to highlight regions that people are likely to look at first. The saliency map is used to highlight the particular areas that people are most likely to look at and it is based on visual distinctness and surprise, can assist in driving a near-optimal initial contour of objects in an input image. The concept of saliency map has been incorporated into other existing studies' models, such as the saliency driven region-edge based top-down level set evolution (SDREL) by Zhi and Shen [23] which has been shown to produce better and more accurate segmentation results. However, the SDREL model is inefficient at segmenting images with significant intensity heterogeneity. Therefore, Iqbal *et al.* [22] developed the local saliency fitting (LSF) by combining the saliency map with the local intensity idea. These two models were designed to segment all objects in the given grayscale and vector-valued images. However, neither of these models is designed to segment a specific object in an input image.

In general, the above-mentioned models can be classified as global ACMs which can be used for segmenting all objects in an input image. In contrast, selective segmentation attempts to segment a targeted object with minimal user intervention. There is enormous potential in applying this technique in tandem with the fields of medical imaging [24], [25] and biometric identification [26]. Several ACM based selective

segmentation models have been formulated to segment colour images. Colour or vector-valued feature is an important aspect in image processing because it carries information that is often critical for understanding and interpreting an image in the domain of the computer vision [27]. Nguyen *et al.* [28] proposed the state-of-the-art interactive image segmentation (IIS) model which uses two sets of geometric constraints and is capable of selectively segmenting vector-valued images. Recently, Ghani and Jumaat [29] proposed a new variational selective model for colour images termed distance selective segmentation 2 (DSS2) model where it uses one geometric constraint (marker set) to identify the specific region of interest. The segmentation result shown was exceptional, but it increases the computational time because of the complexity of the model formulation. Due to that, Jumaat *et al.* [27] modified the DSS2 model into a less complex formulation named the selective segmentation via Gaussian regularization (SSGR) model where the Gaussian regularization term is used in substitution of the total variation (TV) term following the idea from [20]. However, these existing ACM based selective segmentation seem to need making a better initial guess especially for intensity inhomogeneity colour images with sophisticated shapes.

Thus, in this research, we propose a novel variational selective region-based ACM for non-homogeneous intensity vector-valued images by combining the LSF model's local image fitting concept [22] with the saliency image map idea [22], [23]. The other part of this manuscript is organised manner: section 2 summarizes relevant studies as well as the development structure of the proposed model. Section 3 compares the data of the segmentation outcomes and section 4 offers the conclusion and discussion for prospective study.

## 2. METHOD

The incorporation of LSF model [22] and the saliency image map by using the absorbing Markov chain model [30] is formulated to create a minimization novel energy functional for the image segmentation. We note that the utilization of the local image fitting energy is essential when segmenting intensity inhomogeneity images. Figure 1 shows the proposed model's development.

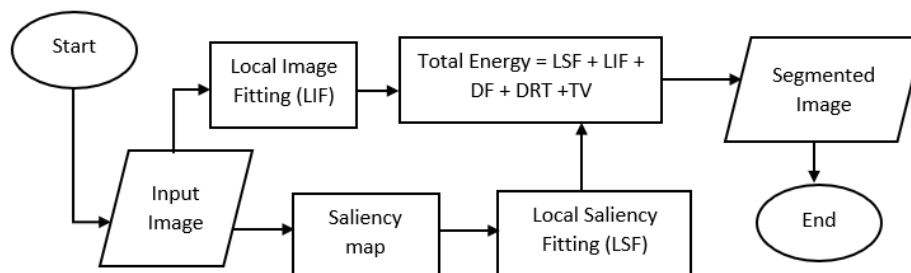


Figure 1. The flowchart of the proposed model's development

Based on Figure 1, a colour input image will be examined. The technique of computing the LIF energy of an input image and the LSF energy from the saliency map energy functional follows. These energies are used with the distance function (DF), the distance regularization term (DRT) and the length term (TV) to generate a total energy functional which aid in the segmentation of images. Each of these processes is explained in depth in the next subsection.

### 2.1. Input image

This experiment includes the partition of 30 test images from diverse sources, 14 of which are medical and 16 of which are synthetic. To meet the research aims, all of the test photos were purposefully chosen based on the intensity inhomogeneity characteristics identified in the images. The ground truth segmentation solutions for all of the test images originated from the same source. All the test images are colour images in the red, green, and blue (RGB) colour space.

### 2.2. Saliency-based functional map via absorbing Markov chain

The process of identifying the most important and visually distinctive regions in an input image is called saliency detection. One of the popular approaches for saliency detection is to use an absorbing Markov chain [30]. An absorbing Markov chain is a mathematical model used to describe a system that moves

through a series of nodes over time. In this case, the states represent different locations or regions within an image. The chain is called absorbing because it includes one or more nodes that, once reached, cannot be left. These absorbing nodes represent the most salient regions.

The absorbing Markov chain involves two nodes: absorbing nodes,  $r$  and the transient nodes,  $t$ . The absorbing nodes represent the salient regions while the non-absorbing nodes represent the background or less important areas. Think about representing node probabilities in a matrix format. Given the assumption that the probability of transition between transient nodes is represented by matrix  $J$ , the probabilities of transition from transient nodes to absorbing nodes is represented by matrix  $K$  while  $I$  is the identity matrix. As a result, the formulation of the transition matrix  $TM$  is expressed as in (1):

$$TM \rightarrow \begin{pmatrix} J & K \\ 0 & I \end{pmatrix} \quad (1)$$

The process begins by converting an image into a graph, where the nodes represent regions of the image, and the edges represent the relationship between them. After that, assign transition probabilities to the edges based on the similarity between the regions they connect. The absorbed time for each transient state can be computed as in (2):

$$y = MO \times f \quad (2)$$

Here, matrix  $f$  denotes the  $t$ -dimensional column vector with elements equal to 1, while matrix  $MO$  signifies what is known as the basic matrix of the absorbing Markov chain and it is given by:

$$MO = (I - J)^{-1} \quad (3)$$

Finding the areas of the image that stands out the most visually is the next step. These areas will act as the Markov chain's absorbing states. This can be done by using the theories of the absorbing Markov chain. The transition probabilities are then changed so that the self-loop probability for the absorbing states is 1, which indicates that once the chain reaches one of these states, it cannot leave. Jiang *et al.* [30] claim that normalizing the absorbed time in (2) produces the saliency map,  $S$  as in (4):

$$S(i) = \bar{y}(i) \quad (4)$$

### 2.3. Local image fitting

The LIF model designed by Zhang *et al.* [20] is a method for image segmentation that utilizes local image fitting functional which is essential to handle intensity inhomogeneity images in order to separate objects in an input image. For any grayscale images  $u(x, y)$  in a domain  $\Omega$ , the regularized local image fitting functional in the level set formulation can be defined as:

$$E_\varepsilon^{LIF}(\phi) = \frac{1}{2} \int_\Omega \left| u - \left( n_1 H_\varepsilon(\phi) + n_2 (1 - H_\varepsilon(\phi)) \right) \right|^2 d\Omega \quad (5)$$

Here,  $H_\varepsilon(\phi)$  represents the Heaviside function such that  $H_\varepsilon(\phi) = 0.5(1 + (2/\pi)\arctan(\phi/\varepsilon))$  while  $n_1$  and  $n_2$  are the intensity averages for the interior and exterior in a local region. Since we are extending the study on segmenting colour images, hence, the (5) can be transformed into the following (6):

$$E_\varepsilon^{LIF}(\phi) = \frac{1}{2} \int_\Omega \frac{1}{N} \sum_{i=1}^N \left[ u^i - \left( m_1^i H(\phi) + m_2^i (1 - H(\phi)) \right) \right]^2 d\Omega \quad (6)$$

Here,  $u^i = u^i(x, y)$  is the  $i^{th}$  channel of a colour image on  $\Omega$  with  $i = 1, 2, \dots, N$  channels. Since our test images are all in RGB format, hence the value of  $N$  is three. The intensity averages of interior and exterior in a local region can be expressed as functions  $m_1^i = (m_1^1, \dots, m_1^N)$  and  $m_2^i = (m_2^1, \dots, m_2^N)$  and it can be defined by a truncated Gaussian window  $W_k(x, y)$  which have the definition as in (7):

$$\begin{cases} m_1^i = \text{mean} \left( u^i \in (\{(x, y) \in \Omega | \phi(x, y) > 0\} \cap W_k(x, y)) \right) \\ m_2^i = \text{mean} \left( u^i \in (\{(x, y) \in \Omega | \phi(x, y) < 0\} \cap W_k(x, y)) \right) \end{cases} \quad (7)$$

thus, (6) has an ability to segment colour image with intensity inhomogeneity.

#### 2.4. Local saliency fitting

The local saliency fitting model is a computer vision technique employed for the purpose of segmenting an image into meaningful areas by leveraging the local saliency information. Here, we elevated a new equation to compute local saliency fitting (LSF) by combining the idea from (4) and (6):

$$E_{LSF}(\phi) = \frac{1}{2} \int_{\Omega} \frac{1}{N} \sum_{i=1}^N \left[ S^i - \left( s_1^i H(\phi) + s_2^i (1 - H(\phi)) \right) \right]^2 d\Omega \quad (8)$$

where  $S^i(x)$  is the saliency colour map equation obtained from (4) and  $s_1^i$  and  $s_2^i$  are the saliency-based averages intensity mean for the inside and outside of the segmentation contour as per in (7). The saliency map is used to segment the image into regions of similar saliency values so that it enables to make a nearly perfect initial guess to ease the segmentation process.

#### 2.5. Total energy functional

In this particular stage, a new variational selective ACM called the saliency-based selective segmentation for colour images (SBSSC) model is introduced. This proposed model consists of LIF in (6) and LSF in (8). The distance function,  $DF = P_d(x, y)$  is introduced to segment specific object effectively. In addition, the presence of total variation function  $TV = \int_{\Omega} \delta(\phi) |\nabla\phi| dx dy$  is used to produce a smooth curve and the distance regularization term  $DRT = \int_{\Omega} \frac{1}{2} (|\nabla\phi| - 1)^2 dx dy$  is implemented in order to achieve a more stable evolution of the segmentation contour that was developed.

Assuming an image  $u$ , a collection of geometrical points  $n_1 (\geq 3)$  were assumed by the marker set  $B = \{w_j = (x_j^*, y_j^*) \in \Omega, 1 \leq j \leq n_1\}$ . The polygon  $P$  was constructed by using set  $B$ . The Euclidean distance function, denoted as  $P_d(x, y)$  quantifies the relative distance between each point  $(x, y) \in \Omega$  from its closest points of  $(x_p, y_p) \in P$ . Consequently, the integration of the aforementioned concept into the level set formulation results in the development of the SBSSC model and yield:

$$\begin{aligned} \min_{\phi} SBSSC(\phi) = & \frac{1}{2} \int_{\Omega} \frac{1}{N} \sum_{i=1}^N \left[ u^i - \left( m_1^i H(\phi) + m_2^i (1 - H(\phi)) \right) \right]^2 d\Omega \\ & + \frac{1}{2} \int_{\Omega} \frac{1}{N} \sum_{i=1}^N \left[ S^i - \left( s_1^i H(\phi) + s_2^i (1 - H(\phi)) \right) \right]^2 d\Omega \\ & + \theta \int_{\Omega} P_d H(\phi) d\Omega + \nu \int_{\Omega} \delta(\phi) |\nabla\phi| d\Omega + \frac{1}{2} \mu \int_{\Omega} (|\nabla\phi| - 1)^2 d\Omega \end{aligned} \quad (9)$$

where  $\theta$ ,  $\mu$  and  $\nu$  are non-negative parameters to handle the DF, DRT and TV terms respectively. The Euler partial differential equation (EL) is derived to solve the model which is defined as in (10).

$$\begin{aligned} \frac{\delta\phi}{\delta t} = & \delta(\phi) \left[ \frac{1}{N} \sum_{i=1}^N \left[ u^i - \left( m_1^i H(\phi) + m_2^i (1 - H(\phi)) \right) (m_1^i - m_2^i) \right] \right] - \mu \left( \Delta\phi - \nabla \cdot \frac{\nabla\phi}{|\nabla\phi|} \right) \\ & + \delta(\phi) \left[ \frac{1}{N} \sum_{i=1}^N \left[ S^i - \left( s_1^i H(\phi) + s_2^i (1 - H(\phi)) \right) (s_1^i - s_2^i) \right] \right] \\ & - \nu \delta(\phi) \nabla \cdot \frac{\nabla\phi}{|\nabla\phi|} + \delta(\phi) [\theta P_d] \end{aligned} \quad (10)$$

#### 2.6. Steps of algorithm for the proposed selective segmentation model

The solution of (10) was computed using MATLAB R2021a software on a CPU processor with the specification of an Intel® Core TM-i10-1065G7 CPU @ 1.30 GHz and 8 GB RAM. To autonomously discontinue the software's execution, we established the two stopping criteria: a tolerance value  $tol = 1 \times 10^{-5}$  and the maximum iterations number of iterations,  $maxit = 200$ . This research presents the Algorithm 1 for implementing the segmentation procedure of the newly proposed SBSSC model as follows:

##### Algorithm 1. Algorithm for the SBSSC model

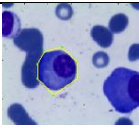
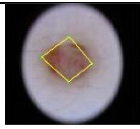
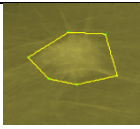
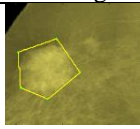
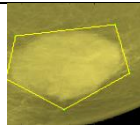
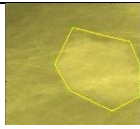
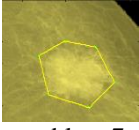
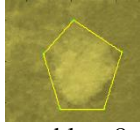
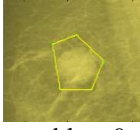
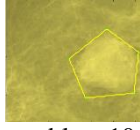
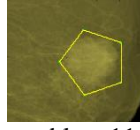
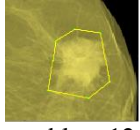
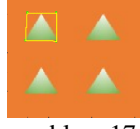
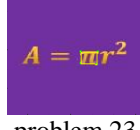
1. Input the vector-valued test image.
2. Set the parameters values of  $\mu$ ,  $\theta$ ,  $\nu$ , tolerance  $tol$ , maximum iterations,  $maxit$  and define the marker set.
3. Compute the saliency map,  $S$  from (4).
4. For  $iteration = 1$  to maximum iterations,  $maxit$  or  $\|\phi^{n+1} - \phi^n\| / \|\phi^n\| \leq tol$  do
5. Evolve the level set function  $\phi$  based on (10).
6. Compute the output  $\phi$  and it is defined as the final solution.

### 3. RESULTS AND DISCUSSION

The proposed SBSSC model's effectiveness was measured against that of some established standards, including the IIS model from Nguyen *et al.*, [28], DSS2 model [29] and the SSGR model [27]. Index similarities namely the dice (DSC) and jaccard (JSC) coefficients will be computed to evaluate the reliability of all segmentation models. In addition, we will calculate the accuracy and error metrics for each model based on how well their segmentation results match the ground truth images. The proximity of the actual segmentation findings to the truth will be indicated by the error measurements. These coefficients will be calculated by comparing the segmentation results of the models with a benchmark value. A coefficient value closer to 0 indicates a poor-quality segmentation, while a value closer to 1 indicates a nearly perfect segmentation. These values differ from error measures where the closer value to 0 indicates a better segmentation result.

In order to get an ideal segmentation result for every model, the parameters involved in the computation have to be set and adjusted manually and thoroughly. Based on how well each test image works with the given segmentation models, a different value of the parameter  $\theta$  is chosen from the range of  $\theta = [3.20000]$ . After that, the parameter  $\nu$  is set in between  $\nu = [10.2500]$  while keeping the parameter  $\mu = 0.001$  fixed. Once an object is selected in a particular image, the segmentation process begins by adjusting the initial markers so that they not only fairly close to the object but also consistent across all models. Then, the markers will automatically connect with each other and form a yellow-edge polygon. There are 30 sample images that were used in this experiment. All the 30 test images with their own markers and initial contour (yellow-edge polygon) are illustrated as shown in the following Table 1.

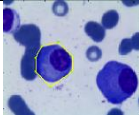
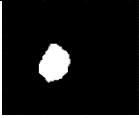
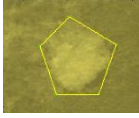
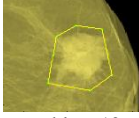
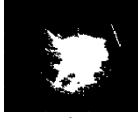
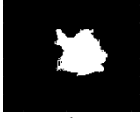
Table 1. Test images with markers and initial contour

Medical and synthetic images					
					
problem 1	problem 2	problem 3	problem 4	problem 5	problem 6
					
problem 7	problem 8	problem 9	problem 10	problem 11	problem 12
					
problem 13	problem 14	problem 15	problem 16	problem 17	problem 18
					
problem 19	problem 20	problem 21	problem 22	problem 23	problem 24
					
problem 25	problem 26	problem 27	problem 28	problem 29	problem 30

Based on Table 1, the first 14 test images are medical images indicated from Table 1 (problem 1 to problem 14) while the remaining 16 test images are synthetic images indicated by Table 1 (problem 15 to problem 30). Table 1 (problem 1) is plasma cell which is obtained from [31] while Table 1 (problem 2) is a skin lesion database obtained from [32]. Table 1 (problem 3 to problem 12) are mammogram images and obtained from INbreast database [29] and [33]. Table 1 (problem 13 and problem 14) are obtained from [34] and images Table 1 (problem 15 to problem 30) are all self-generated synthetic images. The ground truth solutions for each test image were taken from the same source. To provide visual representation, we have chosen six test images (out of the 30 test images) to illustrate the segmentation results for the proposed

SBSSC model and the other existing models as demonstrated in the following Table 2. The complete segmentation results for each of the 30 test images will be presented quantitatively in Table 3.

Table 2. Segmentation results for the chosen six test images

Input images with initial contour	IIS model	DSS2 model	SSGR model	SBSSC model
 problem 1	 a	 b	 c	 d
 problem 8	 e	 f	 g	 h
 problem 12	 i	 j	 k	 l
 problem 25	 m	 n	 o	 p
 problem 28	 q	 r	 s	 t
 problem 30	 u	 v	 w	 x

As shown in the first column of Table 2, we have chosen problem 1, problem 8, problem 12, problem 25, problem 28 and problem 30 to visually illustrate the segmentation performance of all models. It is illustrated that all the models are able to partition the targeted object in each test image. However, there are some results from the DSS2 and SSGR models that produced unnecessary noise as observed in the binary images in Table 2(f), Table 2(g), Table 2(j) and Table 2(k). Furthermore, the DSS2 and SSGR models are incapable of producing good segmentation results when segmenting intensity inhomogeneity synthetic images as illustrated in the binary images Table 2(n), Table 2(o), Table 2(r) and Table 2(s) as both of the models missed to capture the targeted object since the intensity of the targeted object is almost similar to the background. This is not the case for SBSSC model because of the presence of the local intensity and saliency map fittings in the model formulation which considers the local variations in intensity within an image.

Most of the cases especially in medical industries where images are acquired with varying lighting conditions which might lead to image with intensity inhomogeneity issues. Thanks to the local image fitting and saliency map fitting ideas in the formulation which helps to achieve a combination of a smooth background intensity and a spatially varying shading function that captures the local variations in intensity. Once the local intensity variations have been adjusted, the segmentation process becomes easier as the bias in the intensity values have been reduced.

On the other hand, for the IIS model, it somehow unable to identify the targeted object to be segmented as shown in the binary images in Table 2(m) and Table 2(q). This is because according to the authors [28], as the model was formulated as hard segmentation type, it is unable to segment images with sophisticated and fine shapes. Unlike SBSSC model where it applies the absorbing Markov Chain based saliency image map idea in the formulation where it helps to make an outstanding initial guess for the targeted object in an input image especially when the image has different intensity values. In order to support the claims above, we present the average quantitative metrics for the SBSSC model and the three existing models in segmenting all 30 test images in Table 3.

Table 3. The average quantitative metrics for 30 test images for all models

Test Images	14 Medical images	16 Synthetic images	Average
IIS model			
DSC/JSC/	0.8859/0.7986/	0.7459/0.6424/	0.8159/0.7205/
Accuracy/Error	0.9684/0.0316	0.9600/0.0400	0.9642/0.0358
DSS2 model			
DSC/JSC/	0.8853/0.7980/	0.7956/0.6979/	0.8405/0.7480/
Accuracy/Error	0.9672/0.0328	0.9834/0.0166	0.9753/0.0247
SSGR model			
DSC/JSC/	0.8842/0.7961	0.7935/0.6968/	0.8389/0.7465/
Accuracy/Error	0.9668/0.0332	0.9832/0.0168	0.9750/0.0250
SBSSC model			
DSC/JSC/	<b>0.9230/0.8581/</b>	<b>0.9174/0.8643/</b>	<b>0.9202/0.8612/</b>
Accuracy/Error	<b>0.9775/0.0225</b>	<b>0.9939/0.0062</b>	<b>0.9857/0.0143</b>

Based on Table 3, the quantitative results for all the test images have shown that the SBSSC model has the most prevalent average DSC and JSC values. For the average DSC value, the SBSSC recorded 0.9202 which is 12.78%, 9.48% and 9.69% higher than the IIS, DSS2 and SSGR models. In line with the average JSC value, the SBSSC recorded 0.8612 which is 19.53%, 15.13% and 15.37% higher than IIS, DSS2 and SSGR models. In addition, the SBSSC had recorded the highest average accuracy metrics of 0.9857 which is 2.23%, 1.10% and 1.07% higher than the IIS, DSS2 and SSGR models respectively. Since the SBSSC recorded the highest average accuracy metric, the error metric of the model is automatically becoming the lowest. With all of these quantitative accuracy measurements, it is concluded that the SBSSC model is more accurate than the IIS, DSS2 and SSGR models owing to the Markov chain saliency based functional and the local image fitting idea inherent in the SBSSC model's formulation.

Although the proposed SBSSC model provides the highest accuracy compared to other models when partitioning images with intensity inhomogeneity, the SBSSC has its own efficiency limitations. According to the results of the experiment, the SBSSC model had the longest average processing time of 16.8511 seconds, followed by the DSS2 model at 6.1858 seconds and the SSGR model at 0.7080 seconds. From the result, we can observe a huge difference in terms of the average processing time between the SBSSC model and the other models. The average time processing for the IIS model is unknown as the provided IIS software by the authors [31] does not have any tools to record time processing. It is understood that the reason of the SBSSC took longer time to process is mainly because of the existence of the Markov chain saliency-based term and the local image fitting idea together with the total variation (TV) term that make the formulation become a bit complicated compared to the other existing models. Hence, it significantly increases the computational time.

#### 4. CONCLUSION

The underlying goal of this study is to create a unique selective segmentation model that can partition colour images with non-homogeneous colour intensity. Our proposed model, the saliency-based selective segmentation for colour images (SBSSC) model, incorporates the concept of the saliency image map by employing the absorbing Markov chain, which aids in the segmentation process to make an excellent initial guess, and the local image fitting idea, which aids in dealing with various intensities of a particular image. The image segmentation procedure is optimised using the Euler equation, which is then solved and used in MATLAB. In terms of accuracy and efficiency, the SBSSC model's performance is compared to that of other existing models. The segmentation results show that despite having the longest execution time, the SBSSC model has the highest level of accuracy among other comparing models. The SBSSC model is therefore recommended for segmenting colour images, particularly those having intensity inhomogeneity characteristics. Our work also has important implications and real-world applications in a variety of fields. As an illustration, our discoveries can help with object detection and the segmentation process, enabling more precise analysis and diagnosis in medical imaging. Accurate segmentation can provide insights that enable improved analysis and more precise decision making. Our work establishes the foundation for investigating multi-approach image segmentation methods, incorporating our model into more intricate frameworks, and creating real-time segmentation methods in the near future.

#### ACKNOWLEDGEMENTS

Authors express their gratitude to the GIP Research Grant (Project's code: 600-RMC/GIP 5/3 (078/2022)) from Universiti Teknologi MARA, Shah Alam for their valuable support in conducting this

research. Furthermore, the APC was covered by funding from the Pembiayaan Yuran Penerbitan Artikel (PYPA), part of the Tabung Dana Kecemerlangan Pendidikan (DKP), Universiti Teknologi MARA (UiTM), Malaysia

## REFERENCES

- [1] F. A. Shewajo and K. A. Fante, "Tile-based microscopic image processing for malaria screening using a deep learning approach," *BMC Medical Imaging*, vol. 23, no. 1, Mar. 2023, doi: 10.1186/s12880-023-00993-9.
- [2] A. M. Anter and L. Abualigah, "Deep federated machine learning-based optimization methods for liver tumor diagnosis: A review," *Archives of Computational Methods in Engineering*, vol. 30, no. 5, pp. 3359–3378, Mar. 2023, doi: 10.1007/s11831-023-09901-4.
- [3] S. Srinivasan, P. S. M. Bai, S. K. Mathivanan, V. Muthukumar, J. C. Babu, and L. Vilcekova, "Grade classification of tumors from brain magnetic resonance images using a deep learning technique," *Diagnostics*, vol. 13, no. 6, p. 1153, Mar. 2023, doi: 10.3390/diagnostics13061153.
- [4] Z. Q. Habeeb, B. Vuksanovic, and I. Q. Al-Zaydi, "Breast cancer detection using image processing and machine learning," *Journal of Image and Graphics (United Kingdom)*, vol. 11, no. 1, pp. 1–8, Mar. 2023, doi: 10.18178/joig.11.1.1-8.
- [5] I. Mishra, K. Aravinda, J. A. Kumar, C. Keerthi, R. Divya Shree, and S. Srikumar, "Medical imaging using signal processing: A comprehensive review," in *Proceedings of the 2nd International Conference on Artificial Intelligence and Smart Energy, ICAIS 2022*, Feb. 2022, pp. 623–630, doi: 10.1109/ICAIS53314.2022.9742778.
- [6] A. K. Jumaat, W. E. Z. W. A. Rahman, A. Ibrahim, and R. Mahmud, "Segmentation and characterization of masses in breast ultrasound images using active contour," in *2011 IEEE International Conference on Signal and Image Processing Applications, ICSIPA 2011*, Nov. 2011, pp. 404–409, doi: 10.1109/ICSIPA.2011.6144126.
- [7] A. K. Jumaat *et al.*, "Performance comparison of Canny and Sobel edge detectors on Balloon Snake in segmenting masses," Jun. 2014, doi: 10.1109/ICCOINS.2014.6868368.
- [8] M. I. Yeşil and S. Göncü, "Recognition of hereford and simmental cattle breeds via computer vision," *Iranian Journal of Applied Animal Science*, vol. 13, no. 1, pp. 21–32, Mar. 2023, [Online]. Available: [https://ijas.rasht.iau.ir/article\\_699902.html](https://ijas.rasht.iau.ir/article_699902.html).
- [9] K. Jumaat, A. K. Chen, "Three-dimensional convex and selective variational image segmentation model," *Malaysian Journal of Mathematical Sciences*, vol. 14, no. 3, pp. 437–450, 2020.
- [10] G.-L. Zhu, X.-G. Lv, F. Li, and X.-M. Sun, "Nonconvex variational approach for simultaneously recovering cartoon and texture images," *Journal of Electronic Imaging*, vol. 31, no. 04, Jul. 2022, doi: 10.1117/1.jei.31.4.043021.
- [11] X. Liu, G. Liu, Y. Wang, G. Li, R. Zhang, and W. Peng, "A variational level set image segmentation method via fractional differentiation," *Fractal and Fractional*, vol. 6, no. 9, p. 462, Aug. 2022, doi: 10.3390/fractalfract6090462.
- [12] J. W. Soh and N. I. Cho, "Variational deep image restoration," *IEEE Transactions on Image Processing*, vol. 31, pp. 4363–4376, 2022, doi: 10.1109/TIP.2022.3183835.
- [13] S. S. Yasiran *et al.*, "Microcalcifications segmentation using three edge detection techniques," in *International Conference on Electronic Devices, Systems, and Applications*, Nov. 2012, pp. 207–211, doi: 10.1109/ICEDSA.2012.6507798.
- [14] M. Kass, A. Witkin, and D. Terzopoulos, "Snakes: Active contour models," *International Journal of Computer Vision*, vol. 1, no. 4, pp. 321–331, Jan. 1988, doi: 10.1007/BF00133570.
- [15] S. Soomro, A. Munir, and K. N. Choi, "Fuzzy c-means clustering based active contour model driven by edge scaled region information," *Expert Systems with Applications*, vol. 120, pp. 387–396, Apr. 2019, doi: 10.1016/j.eswa.2018.10.052.
- [16] D. Mumford and J. Shah, "Optimal approximations by piecewise smooth functions and associated variational problems," *Communications on Pure and Applied Mathematics*, vol. 42, no. 5, pp. 577–685, Jul. 1989, doi: 10.1002/cpa.3160420503.
- [17] T. F. Chan and L. A. Vese, "Active contours without edges," *IEEE Transactions on Image Processing*, vol. 10, no. 2, pp. 266–277, 2001, doi: 10.1109/83.902291.
- [18] T. F. Chan, B. Yezrielev Sandberg, and L. A. Vese, "Active contours without edges for vector-valued images," *Journal of Visual Communication and Image Representation*, vol. 11, no. 2, pp. 130–141, Jun. 2000, doi: 10.1006/jvci.1999.0442.
- [19] C. Li, C. Y. Kao, J. C. Gore, and Z. Ding, "Implicit active contours driven by local binary fitting energy," Jun. 2007, doi: 10.1109/CVPR.2007.383014.
- [20] K. Zhang, H. Song, and L. Zhang, "Active contours driven by local image fitting energy," *Pattern Recognition*, vol. 43, no. 4, pp. 1199–1206, Apr. 2010, doi: 10.1016/j.patcog.2009.10.010.
- [21] Y. Yang, W. Jia, and B. Wu, "Simultaneous segmentation and correction model for color medical and natural images with intensity inhomogeneity," *Visual Computer*, vol. 36, no. 4, pp. 717–731, Apr. 2020, doi: 10.1007/s00371-019-01651-4.
- [22] E. Iqbal, A. Niaz, A. A. Memon, U. Asim, and K. N. Choi, "Saliency-driven active contour model for image segmentation," *IEEE Access*, vol. 8, pp. 208978–208991, 2020, doi: 10.1109/ACCESS.2020.3038945.
- [23] X. H. Zhi and H. Bin Shen, "Saliency driven region-edge-based top down level set evolution reveals the asynchronous focus in image segmentation," *Pattern Recognition*, vol. 80, pp. 241–255, Aug. 2018, doi: 10.1016/j.patcog.2018.03.010.
- [24] N. F. Idris, M. A. Ismail, M. S. Mohamad, S. Kasim, Z. Zakaria, and T. Sutikno, "Breast cancer disease classification using fuzzy-ID3 algorithm based on association function," *IAES International Journal of Artificial Intelligence*, vol. 11, no. 2, pp. 448–461, Jun. 2022, doi: 10.11591/ijai.v11.i2.pp448-461.
- [25] H. M. Ahmed and M. Y. Kashmola, "A proposed architecture for convolutional neural networks to detect skin cancers," *IAES International Journal of Artificial Intelligence*, vol. 11, no. 2, pp. 485–493, Jun. 2022, doi: 10.11591/ijai.v11.i2.pp485-493.
- [26] A. H. T. Al-Ghraiiri, A. A. Mohammed, and E. Z. Sameen, "Face detection and recognition with 180 degree rotation based on principal component analysis algorithm," *IAES International Journal of Artificial Intelligence*, vol. 11, no. 2, pp. 593–602, Jun. 2022, doi: 10.11591/ijai.v11.i2.pp593-602.
- [27] A. K. Jumaat, R. Nithya, and M. M. Kumar, "Gaussian regularization based active contour model for extraction of shape boundaries in vector valued images," *International Journal of Emerging Technology and Advanced Engineering*, vol. 12, no. 9, pp. 102–112, Sep. 2022, doi: 10.46338/ijetae0922\_11.
- [28] T. N. A. Nguyen, J. Cai, J. Zhang, and J. Zheng, "Robust interactive image segmentation using convex active contours," *IEEE Transactions on Image Processing*, vol. 21, no. 8, pp. 3734–3743, Aug. 2012, doi: 10.1109/TIP.2012.2191566.
- [29] N. A. S. M. Ghani and A. K. Jumaat, "Selective segmentation model for vector-valued images," *Journal of Information and Communication Technology*, vol. 21, no. 2, pp. 149–173, 2022, doi: 10.32890/jict2022.21.2.1.
- [30] B. Jiang, L. Zhang, H. Lu, C. Yang, and M. H. Yang, "Saliency detection via absorbing Markov Chain," in *Proceedings of the IEEE International Conference on Computer Vision*, Dec. 2013, pp. 1665–1672, doi: 10.1109/ICCV.2013.209.

- [31] Ismahan, "Microscopic bone marrow images | Kaggle." Accessed: Nov. 27, 2022. [Online]. Available: <https://www.kaggle.com/datasets/fanouna/microscopic-bone-marrow-images>.
- [32] N. C. F. Codella *et al.*, "Skin lesion analysis toward melanoma detection: A challenge at the 2017 International symposium on biomedical imaging (ISBI), hosted by the international skin imaging collaboration (ISIC)," in *Proceedings - International Symposium on Biomedical Imaging*, Apr. 2018, vol. 2018-April, pp. 168–172, doi: 10.1109/ISBI.2018.8363547.
- [33] I. C. Moreira, I. Amaral, I. Domingues, A. Cardoso, M. J. Cardoso, and J. S. Cardoso, "INbreast: Toward a full-field digital mammographic database.," *Academic Radiology*, vol. 19, no. 2, pp. 236–248, Feb. 2012, doi: 10.1016/j.acra.2011.09.014.
- [34] T. Dietenbeck, M. Alessandrini, D. Friboulet, and O. Bernard, "Creaseg: A free software for the evaluation of image segmentation algorithms based on level-set," in *Proceedings - International Conference on Image Processing, ICIP*, Sep. 2010, pp. 665–668, doi: 10.1109/ICIP.2010.5652991.

## BIOGRAPHIES OF AUTHORS



**Muhammad Syukri Mazlin**    secured his B. Sc. degree in mathematics from Universiti Teknologi MARA (UiTM), Shah Alam. His research interests revolve around mathematical modeling and image processing. At present, he is pursuing M.Sc. degrees in mathematics at School of Mathematical Sciences, College of Computing, Informatics and Mathematics, UiTM, specifically on mathematical imaging techniques. He can be contacted at email: syukri.work03@gmail.com.



**Abdul Kadir Jumaat**    obtained the B.Sc. and M.Sc. degrees in mathematics from the Universiti Teknologi MARA (UiTM), Shah Alam, Malaysia and the University of Liverpool, in United Kingdom, awarded him a Ph.D. degree particularly in applied mathematics (mathematical imaging methods). Presently, he holds the position of senior lecturer at the School of Mathematical Sciences, College of Computing, Informatics and Mathematics and a research fellow at the Institute for Big Data Analytics and Artificial Intelligence (IBDAAI) in UiTM Shah Alam, Malaysia. His research interests encompass various fields such as image/signal processing, artificial intelligence, computer vision, biometrics, medical image and analysis, and pattern recognition. His email address is [abdulkadir@tmsk.uitm.edu.my](mailto:abdulkadir@tmsk.uitm.edu.my).



**Rohana Embong**    received the B. Sc degree in mathematics from Iowa State University, Iowa, United States of America and the M. Sc in Pure Mathematics from UMIST and the Victoria University of Manchester, Manchester, United Kingdom. She is presently an Associate Professor at the School of Mathematical Sciences, College of Computing, Informatics and Mathematics, UiTM, Shah Alam, Malaysia. Her research interests include image processing and fuzzy mathematics. She can be reached at email: [rohana@fskm.uitm.edu.my](mailto:rohana@fskm.uitm.edu.my).